# Radiative proton capture cross sections in the mass range 40–54

Dipti Chakraborty,[*] Saumi Dutta,[†] G. Gangopadhyay,[‡] and Abhijit Bhattacharyya[§]
*Department of Physics, University of Calcutta, 92 Acharya Prafulla Chandra Road, Kolkata-700009, India*
(Received 26 November 2015; revised manuscript received 11 May 2016; published 13 July 2016)

Proton capture cross sections in the energy range of astrophysical interest for mass region 40–54 have been calculated in the Hauser-Feshbach formalism with the reaction code TALYS1.6. The density-dependent M3Y effective nucleon-nucleon interaction folded with target radial matter densities from the relativistic mean field approach is used to obtain the semimicroscopic optical potential. A definite normalization of potential well depths has been used over the entire mass region. The $(p,\gamma)$ rates of some reactions, important in the astrophysical scenario, are calculated using the potential in the relevant mass region.

DOI: 10.1103/PhysRevC.94.015802

## I. INTRODUCTION

During stellar burning, reactions involving different seed nuclei assume importance at different temperature and burning zones. The seeds in the concerned mass range $A = 40$–$54$ are mainly produced during hydrostatic carbon burning and explosive oxygen burning. These then take part in synthesizing more massive elements via various reactions occurring in later phases of evolution [1,2].

The principle energy-generating processes in stars, i.e., the $pp$-cycle, CNO cycle, HCNO cycle, $rp$-process, etc., are reactions which require continuous addition of protons against the Coulomb barrier. Certain astrophysical sites, such as x-ray bursters, involve high flux of protons at temperatures of ∼several GK and matter density $\sim 10^6$ g/cc that initiate a rapid proton capture process which ultimately results in a thermal burst of very short duration, peaked in the x-ray regime. Knowledge of the cross sections, and equivalently, the rates of the reactions occurring in these sites are required to study complete nucleosynthesis via a network calculation. However, it is difficult to measure all the essential rates in terrestrial laboratories due to the unavailability and instability of the required targets. Reaction rates calculated in a theoretical approach may provide the necessary information in this context after proper validation of theory with the experimental data. For abundance calculations in an explosive astrophysical environment, the concerned network must have to take into account various quantities such as temperature, pressure, and proton mass fraction, along with forward and reverse reaction rates. So, we need to take care of the proper tuning of the interaction potential.

Many works have been devoted so far to the study of theoretical capture cross sections by constructing different nucleon-nucleus potentials. Rauscher *et al.* [3,4] have calculated reaction rates in a global approach and suggested that statistical model calculations can be improved using locally tuned nuclear properties like optical potential. Reaction rates from the phenomenological approach, i.e, with phenomenological global optical potentials or even with semimicroscopic optical potential with phenomenological densities, give rise to uncertainty and the reaction rates have to be varied by large factors to study their effects. Prediction of rates, as has been done in Ref. [5], gave rise to uncertainties away from the stability valley. Phenomenological global optical potential should not be expected to provide an adequate description of nucleon-nucleus interaction, because differences in nuclear structure among adjacent nuclei do not allow simple and smooth $Z$ and $A$ dependence of the Woods-Saxon parameters. Microscopic optical potentials obtained by folding with appropriate microscopic densities are expected to be more accurate and do not require frequent variation of the reaction rates. On the other hand, calculation of reaction rates in a microscopic or semimicroscopic with microscopic density prescription approach is far more free from these uncertainties. Recently, the semimicroscopic optical potential obtained in a folding model prescription has proved to be highly successful in explaining various nuclear phenomena. For example, Bauge *et al.* [6,7] constructed a lane-consistent semimicroscopic optical potential to study elastic scattering and differential and total cross sections for nuclei over a broad mass range. The theoretical cross-section calculation requires a complete knowledge of various ingredients such as transmission coefficients, i.e., transition probabilities (averaged over resonances of the compound nucleus formed upon radiative proton captures) between various states which in turn depend on the level schemes, lifetimes of the states, level densities, $\gamma$-ray strength functions, nuclear masses, giant dipole resonance parameters, etc.

Application of a statistical model requires sufficiently high nuclear level density in the compound nuclear state. The theoretical reactions are generally derived in the Hauser-Feshbach (HF) formalism which assumes the presence of a sufficiently large number of resonances at relevant energies. The cross sections are in general the sum of contributions from different reaction mechanisms depending on projectile energies. At higher energies, the presence of many close and overlapping resonances allow one to calculate an average cross section using the HF approach. Sometimes there are interference effects between single resonance and direct capture. The nonresonant reaction cross sections are mainly determined by the direct capture transitions to the ground states and

[*]diptichakraborty2011@gmail.com
[†]saumidutta89@gmail.com
[‡]ggphy@caluniv.ac.in
[§]abhattacharyyacu@gamil.com

 

low excited states. In light nuclei and low energy regimes, level densities are generally low, especially for targets near closed shells with widely spaced nuclear levels and close to drip lines with low particle separation energies and $Q$ values. Hence, application of a statistical model to these nuclei at astrophysical temperatures is somewhat problematic and requires careful study.

Optical potential is a very important ingredient in HF statistical model calculations. Here, we have constructed an optical potential by folding the density-dependent M3Y (DDM3Y) interaction with the densities of the target. The DDM3Y interaction has proved to be successful in explaining various nuclear properties. For example, folded DDM3Y nucleon-nucleus interaction potential has been successfully used to study the incompressibility of infinite nuclear matter [8] and radioactivity lifetimes of spherical proton-rich nuclei [9].

The paper is organized as follows. In the next section we present the framework of our calculation. In Sec. III we discuss the results, and in the last section we summarize.

## II. MODEL CALCULATION

Proton capture reactions for nuclei $A \geqslant 40$ have $Q$ values $\geqslant$5 MeV which increase with increasing number of neutrons. We have studied proton capture reactions in several nuclei in the mass range $A = 40$–$54$ in a semimicroscopic HF formalism and compared our results with experiments. All these nuclei have $Q$ values for proton capture at ground states within $\sim$5 to 10 MeV.

We have calculated the reaction cross sections in the HF approach using the folding model formalism with the TALYS1.6 code [10]. The code TALYS incorporates much more physics than other codes available previously. It takes care of preequilibrium emission, detailed competition between all open channels, detailed width fluctuation correction, coherent inclusion of fission channel, coupled channel calculation for deformed nuclei, multiparticle emission etc. Details can be found in the TALYS1.6 manual. Along with these advantages of the code, the code can be used with fully microscopic inputs and hence is suitable for determination of unknown rates, a feature utilized in the present calculation. The present approach scores out the phenomenological method of Goriely *et al.* [11] with the same code. The HF formalism generally considers the formation of a compound nuclear state. The present method has been adopted in a number of our recent works [12–17]. Radial densities have been obtained from relativistic mean field (RMF) approach using the FSUGold Lagrangian density [18], details of which are given in Refs. [19,20]. The target is assumed to be spherical and calculations are done in coordinate space. Considering the finite size of the proton, charge densities are obtained by convoluting the point proton density with a standard Gaussian form factor $F(\mathbf{r})$ [21],

$$\rho_{\rm ch}(\mathbf{r}) = e \int \rho(\mathbf{r}')F(\mathbf{r}-\mathbf{r}')d\mathbf{r}', \tag{1}$$

where

$$F(r) = (a\sqrt{\pi})^{-3} \exp\left(-\frac{r^2}{a^2}\right). \tag{2}$$

Here we have $a = \sqrt{2/3}a_p$, with $a_p = 0.80$ fm being the rms charge radius of the proton. The effect of the center-of-mass correction is neglected while calculating the charge density or radius, because it goes as $A^{-4/3}$, as given in Ref. [22].

The DDM3Y interaction is folded with the radial densities of targets obtained from the RMF approach. This interaction potential is then incorporated into the reaction code. The interaction, in MeV, at a distance $r$ (in fm) is given by [23–25]

$$v(r,\rho,E) = t^{\rm M3Y}(r,E)g(\rho), \tag{3}$$

with the M3Y interaction (including a zero-range pseudopotential) given by [26,27]

$$t^{\rm M3Y} = 7999\frac{e^{-4r}}{4r} - 2134\frac{e^{-2.5r}}{2.5r} - 276\left(1 - 0.005\frac{E}{A}\right)\delta(r), \tag{4}$$

$E$ is the energy in MeV in the center-of-mass frame of the projectile, and $\rho$ is the nuclear density. The density-dependent factor $g(\rho)$ is given as [28]

$$g(\rho) = C[1 - \beta\rho^{2/3}]. \tag{5}$$

The constants $C$ and $\beta$ are assigned values 2.07 and 1.624 fm$^2$, respectively, obtained from nuclear matter calculation [8]. We have further included a spin-orbit term coupled with phenomenological energy-dependent potential depths according to the Sheerbaum prescription [29] as

$$U^{\rm so}_{n(p)}(r) = (\lambda_{\rm vso} + i\lambda_{\rm wso})\frac{1}{r}\frac{d}{dr}\left(\frac{2}{3}\rho_{p(n)} + \frac{1}{3}\rho_{n(p)}\right), \tag{6}$$

where,

$$\lambda_{\rm vso} = 130\exp(-0.013E) + 40, \tag{7}$$

$$\lambda_{\rm wso} = -0.2(E - 20). \tag{8}$$

The DDM3Y interaction potential provides only the real part, and the imaginary part of the optical model potential has been taken to be identical with the real part. The folded potential is then renormalized to obtain reasonable agreement with the experimental data. We have used the same renormalization factor, 0.9, for the entire mass region and have used the same potential for the real and imaginary parts of the potential. The advantage of using the same renormalization factor for the entire mass region is that it ensures that the present method can be extended to nuclei where experimental data are not available.

Nuclear level densities are important ingredients of the calculation [30,31]. We have used Goriely's microscopic results for level density [32] and the Hartree-Fock-Bogoliubov model for the $E1$ $\gamma$-ray strength function [33]. These choices were used in some of our previous calculations also. We always try to avoid too much variation of the theory or input parameters to have easy extrapolation of the rate parameters in future use. Hence, we decided to keep the nuclear level density model the same as in our previous publications in the mass range 55–80 [12–17]. We have checked that this choice works well in the mass region $A = 40$–$80$. Width fluctuation correction, which is due to the retention of some memory of the initial channel, is also important. Though it assumes significance mainly in elastic scattering, it is also important

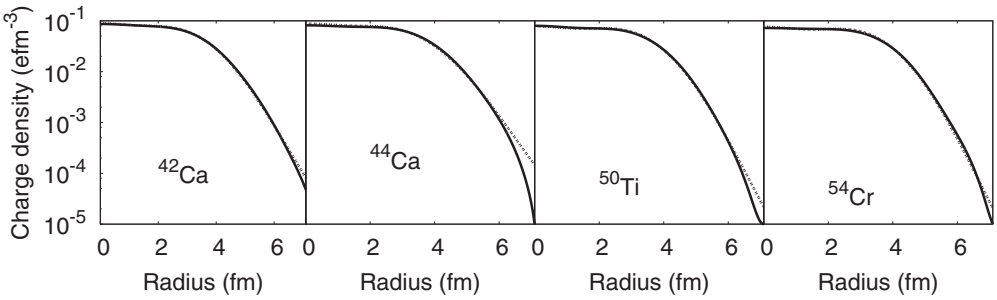


FIG. 1. Density profiles of some nuclei in the mass range of interest. Solid lines denote our results and dashed lines indicate results from the Fourier-Bessel (FB) parametrizations obtained from fitting the experimental data.

near threshold energies, where competition cusps arise due to the existence of different channel strengths.

Nuclear masses, if experimental values are not available, are taken from Ref. [34]. Preequilibrium effects have been included in the cross-section calculation. Thirty discrete levels for both target and residual nuclei have been taken into consideration in the Hauser-Feshbach decay and $\gamma$-ray cascade. Full $j,l$ coupling between the states is considered. The TALYS database includes all these necessary ingredients.

Astrophysical proton capture reactions are mainly important in a definite energy window, termed as the effective Gamow energy window, distributed around the Gamow peak [35]. In charged particle reactions, the window arises from the folding of the Maxwell-Boltzmann distribution of the particles with the Coulomb barrier penetrability. Consequently, rates for charged particle reactions are largely suppressed at both low and high energies. Both the peak energy and the width depend on charges of the projectile and the target and temperature of the astrophysical environment.

Proton capture reaction cross sections have been calculated for energies relevant to this energy window and compared with available experimental data. The relevant Gamow energy window for this mass region lies between 1 and 2 MeV corresponding to the temperature $\sim$2GK. $S$ factors are commonly used in astrophysical applications at such low incident energies where cross sections show strong energy dependence. $S$ factors remove the Coulomb dependence and hence it is a slowly varying function of energy. It is given by

$$S(E) = E\sigma(E)\exp(2\pi\eta). \tag{9}$$

Here $\eta$ is known as Sommerfeld parameter given by

$$\eta = 0.989534\, Z_p Z_t \mu/E. \tag{10}$$

with $\mu = \frac{m_p m_t}{m_p + m_t}$ being the reduced mass; $Z_p$ and $Z_t$ are proton numbers of the projectile and target, respectively, and $m_p$ and $m_t$ are projectile and target masses, respectively.

Finally, we have calculated the rates of some reactions which have been identified as important by Parikh *et al.* [36] in x-ray burst (XRB) nucleosynthesis. They have done post-processing calculations for type I x-ray bursts using ten different models with different temperature density profiles. Three of them are from Koike *et al.* [37], Schatz *et al.* [38], and Fisker *et al.* [39]. They have further parametrized the model of Koike *et al.* to probe the effects of burst peak temperature, burst duration, and metallicities. Using these ten models, they have studied the impacts of thermonuclear reaction rates on XRB yields. They have identified some reactions as important in the mass range of our interest. We have calculated the rates of those reactions with our theoretical model and further compared with the rates predicted by the NON-SMOKER reaction code [40].

## III. RESULTS

### A. RMF calculations

In the present work, the RMF approach is used to obtain density distributions which are then folded with the interaction to obtain the optical potential. We have plotted the charge density profiles of some nuclei in the relevant mass region in Fig. 1 and compared them with experimental values extracted from Fourier-Bessel parametrizations [41]. One can see that our theory can reproduce the experimental density very well. Further, in Table I we have listed the calculated binding energy and charge radii values with the experimental measurements from Refs. [42] and [43], respectively. In case of binding energies the theoretical values have been corrected following the prescription in [44,45]. One can readily see that the agreement between theory and measurement is reasonable with the difference between them less than 1.5%. For charge radii the difference between theory and experiment is less than 2.1% as can be seen from Table I.

### B. Cross-section calculation and astrophysical $S$ factor

Proton capture cross-section data are available for a large number of targets in this mass region. We have calculated the values using our approach and then we compared those with experimental measurements. The cross section for the $^{41}$K$(p,\gamma)^{42}$Ca reaction has been measured using Ge(Li) detectors of volume 125 cm$^3$ below the neutron threshold and 60 cm$^3$ above the neutron threshold by Sevior *et al.* [46]. Theoretical cross sections were calculated with the statistical code HAUSER*4 [47]. Reasonable agreement with experimental values was obtained by reducing the imaginary well depths in global parameters. Our calculation excellently reproduces the measurement as can be seen from Fig. 2 without any further modification.

The only stable isotope of vanadium is $^{51}$V. The $S$ factors for the $(p,\gamma)$ reaction fall steeply above 1.5 MeV of energy due to the low threshold of the $(p,n)$ reaction channel ($Q = -1.534$ MeV), a consequence of neutron richness of $^{51}$V. A competition between these two reaction channels causes a drop in the $(p,\gamma)$ cross section for incident energies just above

TABLE I. Comparison of experimental and calculated binding energy (BE) and charge radii values for all the stable nuclei in the mass range of interest. Theoretical BE values are from RMF with the $N_pN_n$ correction [44,45].

| Nucleus | BE (MeV) | | Charge radius (fm) | | Nucleus | BE (MeV) | | Charge radius (fm) | | Nucleus | BE (MeV) | | Charge radius (fm) | |
|---|---|---|---|---|---|---|---|---|---|---|---|---|---|---|
| | Theory | Expt. | Theory | Expt. | | Theory | Expt. | Theory | Expt. | | Theory | Expt. | Theory | Expt. |
| $^{40}$Ar | 340.36 | 343.81 | 3.36 | 3.42 | $^{41}$K | 351.76 | 351.62 | 3.40 | 3.45 | $^{40}$Ca | 341.90 | 342.05 | 3.43 | 3.47 |
| $^{42}$Ca | 360.80 | 361.89 | 3.43 | 3.50 | $^{43}$Ca | 370.13 | 369.83 | 3.44 | 3.49 | $^{44}$Ca | 375.80 | 380.96 | 3.44 | 3.51 |
| $^{46}$Ca | 395.85 | 398.77 | 3.45 | 3.49 | $^{45}$Sc | 386.85 | 387.85 | 3.48 | 3.54 | $^{46}$Ti | 393.69 | 398.20 | 3.52 | 3.60 |
| $^{47}$Ti | 403.93 | 407.08 | 3.52 | 3.59 | $^{48}$Ti | 414.02 | 418.70 | 3.53 | 3.59 | $^{49}$Ti | 423.59 | 426.85 | 3.53 | 3.57 |
| $^{50}$Ti | 432.34 | 437.78 | 3.53 | 3.57 | $^{51}$V | 441.25 | 445.85 | 3.57 | 3.59 | $^{50}$Cr | 428.69 | 435.05 | 3.60 | 3.66 |
| $^{52}$Cr | 450.07 | 456.35 | 3.60 | 3.64 | $^{53}$Cr | 459.00 | 464.29 | 3.61 | 3.65 | $^{54}$Cr | 467.19 | 474.01 | 3.63 | 3.68 |
| $^{54}$Fe | 464.91 | 471.76 | 3.66 | 3.69 | | | | | | | | | | |

the neutron threshold. This particular low $(p,n)$ threshold in some nuclei is of major importance as it provides opportunity to study both reactions within the range of astrophysically important bombarding energies.

Zyskind *et al.* [48] measured the $^{51}$V$(p,\gamma)^{52}$Cr reaction cross sections. The $\gamma$ rays and neutrons were detected by a 73 cm$^3$ Ge(Li) detector and BF3 long counter, respectively. They also compared the average values of the measured cross section with two theoretical models, the Kellogg global HF program (KGHFP) [49] and HAUSER*4 [47]. They observed that KGHFP overpredicts the measurement by 30–50% while HAUSER*4 exceeds the data by only 2–3%. The errors in their measurement arose mainly from target thickness and detector efficiency resulting in an overall uncertainty of about 20%.

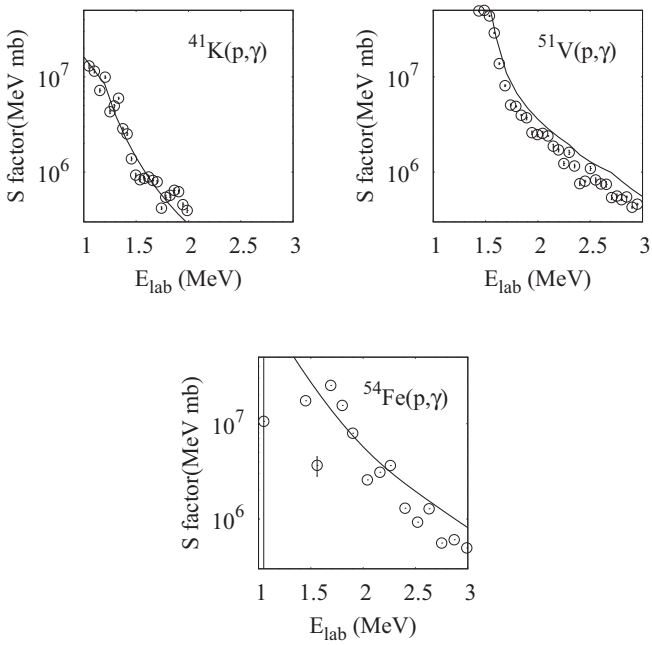


FIG. 2. Comparison of astrophysical $S$ factor with available experimental values for the potassium, vanadium, and iron isotopes. Solid lines denote our present calculation and the discrete points denote experimental values. In most of the cases, errors, when available, are smaller than the dimensions of the points.

The present theory overestimates the measurement by a factor ∼2 as can be seen from Fig. 2.

The Fe isotope with mass number $A = 54$ is an even-even nucleus with a magic neutron number. Kennet *et al.* [50] measured the cross section of the reaction $^{54}$Fe$(p,\gamma)^{55}$Co using a 125 cm$^3$ Ge(Li) detector in the energy range 1.05–3.69 MeV. Those cross sections were obtained by the authors after summing up three major transitions which resulted in 59±3% of the total reaction strength corresponding to the ground state transitions from first, second, and third excited states. The absolute error in their measurement was reported to be of the order of 12%. They carried out a statistical calculation using HAUSER*4 [47] which overestimated the cross section. In search of an improved fit they proposed a new prescription by considering proton imaginary well depth as a free parameter and obtained a best fit linear relationship between the reduced proton imaginary well depth and proton number. However, the experimental data were taken at large energy intervals and are highly scattered making the comparison difficult. Nevertheless, the agreement with our theoretical prediction for this case, if not excellent, is within satisfactory limits as can be seen from the Fig. 2. The value corresponding to the lowest energy has a large error.

One of the stable even-even isotopes of calcium is $^{42}$Ca originated mainly via the explosive oxygen burning in an appropriate stellar environment. This is of some importance in the study of quasiequilibrium achieved during explosive silicon burning and plays a very important role in bridging the chain reactions involving masses $28 \leqslant A \leqslant 45$ with those involving masses $45 \leqslant A \leqslant 62$ [51]. It is also a possible contributor to the $s$-process abundance as it lies along the $s$-process nucleosynthesis path. Proton capture on the $^{42}$Ca isotope produces the relatively long-lived $^{43}$Sc isotope.

Vlieks *et al.* [52] determined the cross section by measuring annihilation photons emitted after positron decay of $^{43}$Sc (half-life = 3.89 h). They compared their measurement with theoretical calculations and found good agreement below 4.5 MeV. The uncertainties in their measurement were mainly from target thickness resulting in an overall uncertainty of 21% below 3 MeV of energy, which further increased to 24% above 3 MeV energy.

Later Mitchell *et al.* [53] measured the same reaction cross section but with a more direct technique with a 125 cm$^3$ Ge(Li)

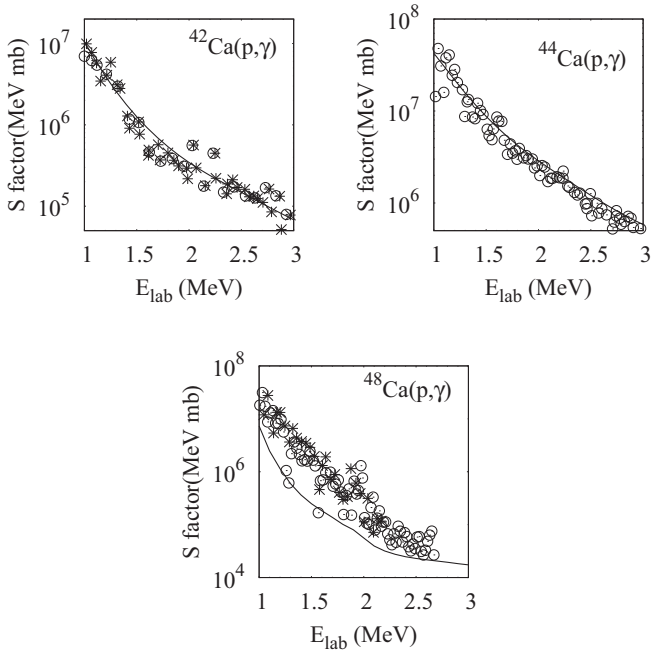


FIG. 3. Same as Fig. 2, but for calcium isotopes.

detector. The total cross section of $^{42}$Ca$(p,\gamma)^{43}$Sc was obtained from the excitation function of the three major $\gamma$ transitions that comprised 65% of total strength. They further compared their measurement with the statistical HAUSER*4 [47] code and found that theoretical prediction was higher by a factor of ∼1.5. They reported the errors associated with their experimental cross sections for this particular reaction to be 18%. Our calculation presents far better agreements with the measurements of both groups than their statistical model calculations, as can be seen from a comparison of the plots in Fig. 3 of this work with Fig. 1 of Ref. [52], and Fig. 5 of Ref. [53].

Mitchell *et al.* [53], in the same work, also measured the cross section of the $^{44}$Ca$(p,\gamma)^{45}$Sc reaction. In the case of $^{44}$Ca, yield was determined from the sum of all spectra feeding the first excited state and the ground state. The selected four of all transitions within 3.0 MeV of bombarding energy, carrying 68% of the total strength were used to determine the total cross section of this reaction. The comparison with the HAUSER*4 prediction resulted in an overall agreement within a factor ∼1.3. This is more or less similar to the agreement with present theory.

The doubly magic nuclei of $^{48}$Ca have a very long half-life against radioactive decay and can be considered as stable for all practical purposes. These nuclei may be produced during explosive carbon burning by reactions of a few neutrons and protons with a small admixture of seed nuclei present at the time of star formation [1]. Being a neutron-rich nucleus, it is very important and can be treated as a starting point of production of new nuclei. Experimental data for this reaction were taken from Refs. [54,55]. The experiment by Kennett *et al.* [54] was carried out using a 60 cm$^3$ Ge(Li) detector with detection efficiency determined *in situ*. The total cross section was determined from the 83±5% contribution of two transitions to the ground state from first and second excited states. The strength was determined from branching ratios averaging over the resonances. Zyskind *et al.* [55] also measured the $(p,\gamma)$ reaction cross section on $^{48}$Ca using a 73 cm$^3$ Ge(Li) detector. The data, even after smoothing, contain considerable fluctuations.

The difference between our theoretical prediction and the experimental data may possibly be attributed to the effect of the doubly magic core of the $^{48}$Ca nucleus. The resonances are few and the level density of the compound nucleus system is quite low also. So, the experimental data contain considerable fluctuations and in such a case, statistical modeling is not expected to be very effective because the HF calculation assumes an average over many resonances. Another important aspect is that due to the low lying states of the residual nucleus of competing $(p,n)$ channels the, $(p,\gamma)$ cross section changes dramatically.

The experimental data for the $(p,\gamma)$ reaction on $^{50}$Cr are taken from Krivonosov *et al.* [56]. The $\gamma$ rays and and $\beta^+$ radiation were detected in coincidence. They determined the cross sections by analyzing principal $\gamma$ rays and annihilation radiation as well as $\beta^+$ radiation. There are large fluctuations in the experimental data, which are rather old too. The present calculation underestimates the average data by a factor of ∼4–5. This, though not very good, is perhaps reasonable for such a work which aims to set a definite set of normalization over an entire mass range. A local tuning of parameters can of course provide more accurate results.

Gardner *et al.* [57] measured the proton capture reactions on $^{53}$Cr. The $\gamma$ rays were detected with a 68 cm$^3$ Ge(Li) detector and the analysis was performed from the five transitions feeding the first excited state (0.054 MeV) and ground state of $^{54}$Mn. The overall accuracy of the measurement was estimated to be 12% with the greatest source of the error resulting from target thickness uncertainty. Statistical model calculations done by the authors using global optical model parameters showed satisfactory agreement with the experiment. Our microscopic theory, however, gives a far better agreement with their measurement, especially below the $(p,n)$ threshold (at 1.40 MeV) where only the $(p,\gamma)$ reaction channel is open.

The experimental data for the $(p,\gamma)$ reaction on $^{54}$Cr target is from Ref. [58]. A 73 cm$^3$ Ge(Li) detector was used to measure the absolute cross section of the reaction. The systematic error was reported to be ∼20%. The experimental excitation function was plotted by the authors along with the results of statistical HF calculations of Ref. [59] and the results from the HAUSER*4 code [47]. They found excellent agreement with Ref. [59]; however, the results from the HAUSER*4 code showed some inconsistencies. We get excellent agreement with the experimental results perhaps better than both the calculations mentioned above as can be seen from Fig. 4.

Some of the Ti isotopes are important in astrophysics. For example, the most strongly deformed even-even Ti nucleus is $^{46}$Ti. It is mainly produced during stellar burning stages in asymptotic giant branch (AGB) stars via rapid capture of protons on the Sc isotope. Traces of it is also observed in some collapsing stars, supernovae, etc. The $^{46}$Ti isotope contributes also to the (though small) $rp$-process flux and to the early burning stages of the x-ray bursts affecting the luminosity of the objects. The $^{46,47}$Ti isotopes carry a dominant flow of nucleosynthesis from the mass 45 bottle neck to the elements of the iron group [51].

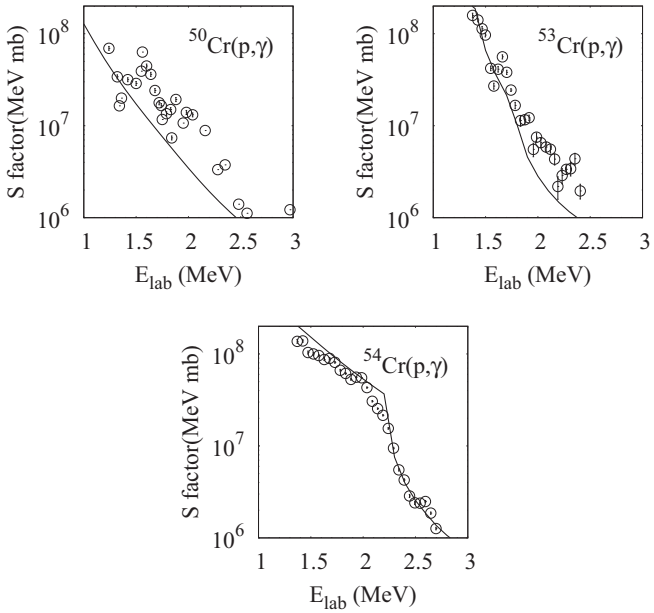


FIG. 4. Same as Fig. 2, but for chromium isotopes.

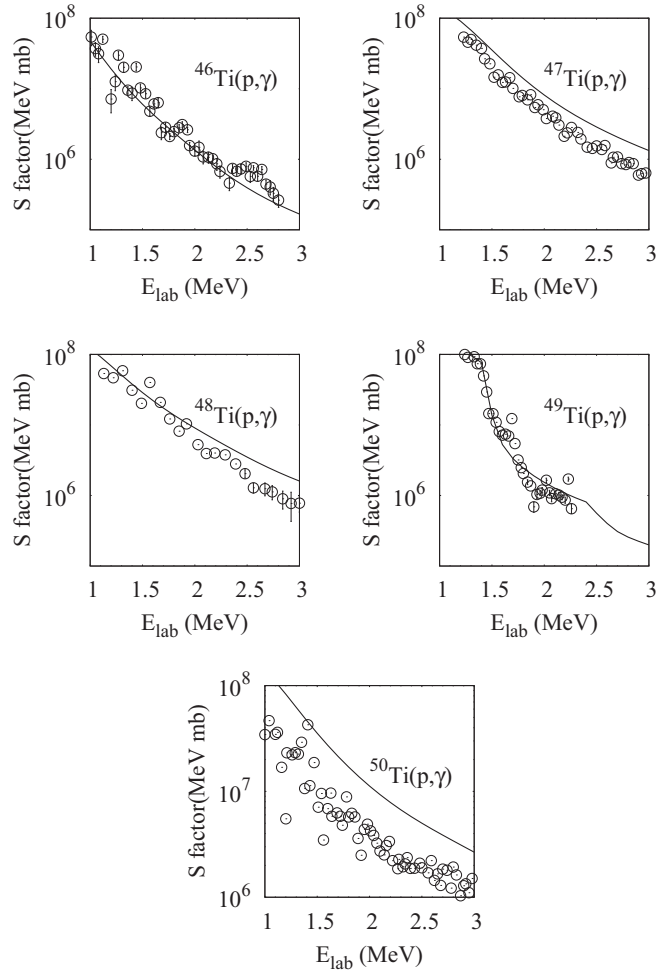


FIG. 5. Same as Fig. 2, but for titanium isotopes.

The experimental cross-section values for $^{46}$Ti$(p,\gamma)^{47}$V, $^{47}$Ti$(p,\gamma)^{48}$V, and $^{48}$Ti$(p,\gamma)^{49}$V reactions are taken from Ref. [60]. The $(p,\gamma)$ reaction yields were measured with a 125 cm$^3$ Ge(Li) detector with efficiencies accurate within $\pm$5%. However, for cross sections above the neutron threshold on $^{47}$Ti a 60 cm$^3$ Ge(Li) detector was used. They determined the cross sections from the selected transitions after summing up all spectra over a wide energy range and correcting for the fraction of intensity belonging to the selected lines. The data were compared with HAUSER*4 code calculations and agreements were within 30%, 50%, and 20% for $^{46}$Ti, $^{47}$Ti, and $^{48}$Ti, respectively, as reported by the authors. The authors concluded that the agreement was good for the globally parametrized statistical code. Our theory reproduces the measurements reasonably well, within a factor of $\sim$1.5 or less, for all three cases. However, in the case of $^{46}$Ti, our result varies by a factor of $\sim$10 with another set of experimental data available in Ref. [61] and the reason for this discrepancy is not very clear.

Kennet *et al.* [62] measured the cross section for the $^{49}$Ti$(p,\gamma)^{50}$V reaction. The $(p,\gamma)$ excitation function was obtained by observing the transition from the first excited state to the ground state of $^{50}$V which is reported to carry 97% of the total $(p,\gamma)$ strength. The authors compared their results with the calculation from the HAUSER*4 code [47] and found agreement within 30%. The present model gives an excellent agreement with experiment for this particular reaction as can be seen from Fig. 5.

The even-even nucleus $^{50}$Ti contains a magic number of neutrons and is the most neutron rich among the five stable isotopes of titanium. The experimental data for proton capture on $^{50}$Ti are from Ref. [63]. The experiment was carried out with a Ge(Li) detector of dimensions 125 cm$^3$ and 60 cm$^3$, below and above the neutron threshold, respectively. A comparison with the results of HAUSER*4 code [47] revealed that the code overestimated the proton transmission coefficient at the entrance channel, resulting in overpredictions by a factor of $\sim$3. Our results also show significant overestimation in the $S$ factor for this reaction. This can perhaps be attributed to the limitation of the statistical model near a closed shell where large shell gaps lead to low level densities.

It is worth noting that the data for radiative proton capture reactions in the astrophysical energy range are scarce. Even most of the existing data are also very old and lack the application of modern techniques. Thus the possibility of the presence of errors associated with the data is high. In most cases individual error associated with each data point is not available. Hence, it is extremely difficult to use these data with much reliability. Our aim is to present a unique set of parametrization over the entire mass range so that the cross section can be extrapolated to those targets for which the data are unavailable todate. We do not expect that our results will need to be modified after any remeasurement of the values.

### C. Astrophysical $(p,\gamma)$ reaction rate calculation

Inside stars, nuclides not only exist in their ground states but also in their excited states and a thermodynamic equilibrium holds to a very good approximation. The assumption of a thermodynamic equilibrium combined with the compound

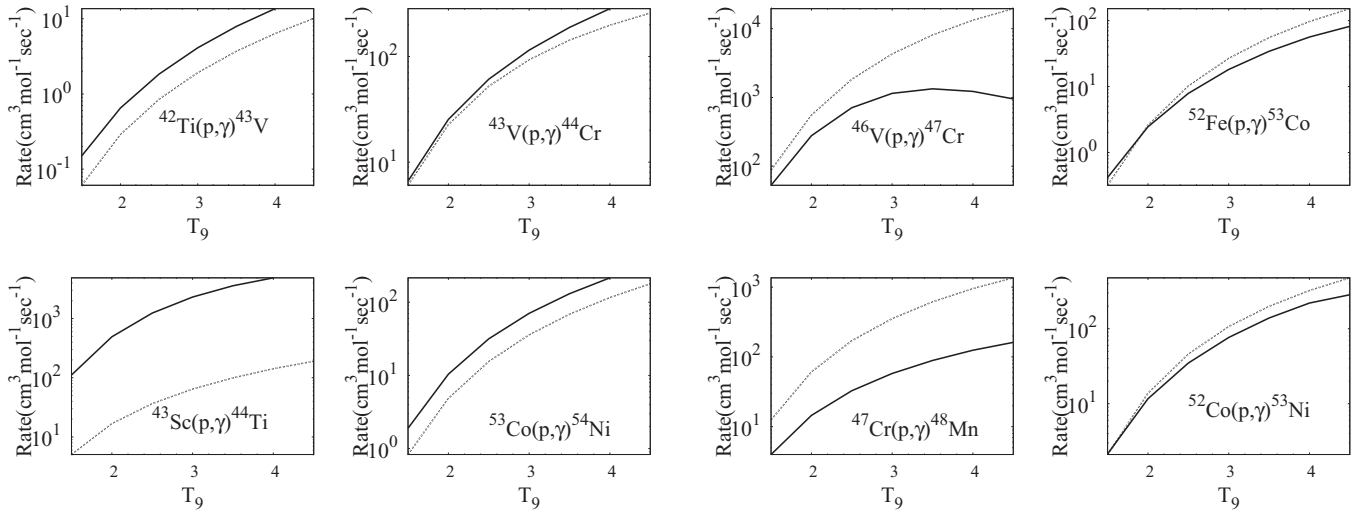


FIG. 6. Comparison of proton capture reaction rate with NON-SMOKER result. Solid line denotes the rates predicted by our calculation and dotted curve denotes the NON-SMOKER result.

nucleus cross sections for the various excited states then allows us to produce Maxwellian averaged reaction rates, which are important inputs for stellar evolution models. In astrophysical environment, e.g., x-ray bursters, the relative populations of levels of target nuclei obey a Maxwell-Boltzmann distribution. The effective stellar rate in the entrance channel at temperature $T$ taking account of the contributions of the various target excited states is expressed as

$$N_A\langle\sigma v\rangle^*_{\alpha\alpha'}(T) = \left(\frac{8}{\pi\mu}\right)^{1/2}\frac{N_A}{(kT)^{3/2}G(T)} \times \int_0^\infty \sum_\nu \frac{(2I^\nu+1)}{(2I^0+1)}\sigma^\nu_{\alpha\alpha'}(E)E \times \exp\left(-\frac{E+E^\nu_x}{kT}\right)dE, \quad (11)$$

where $\nu$ represents various excited states in the nucleus and

$$G(T) = \sum_\nu \frac{(2I^\nu+1)}{(2I^0+1)}\exp\left(-\frac{E^\nu_x}{kT}\right) \quad (12)$$

is the $T$-dependent normalized partition function. Figure 6 shows the reaction rates for the $(p,\gamma)$ reaction from the present calculation being compared with the rates from the NON-SMOKER code [40,64]. The NON-SMOKER code is an improvisation of the well-known reaction code SMOKER [65] with modified level density description, explicit isospin mixing treatment, width fluctuation correction, and giant dipole resonance energies and widths. The NON-SMOKER code uses a HF calculation based on masses from the finite range droplet model (FRDM) [66]. We have plotted the proton capture rates in the temperature range of 1 to 4.5 GK for some reactions in the mass region in Fig. 6 in the cases where our results differ significantly from the NON-SMOKER results. The numerical values of the reaction rates are given in the Supplemental Material [67]. As can be seen, the reaction rates determined from our theory are more than the NON-SMOKER rates for $^{42}$Ti, $^{43}$V, $^{43}$Sc, and $^{53}$Co targets. Our calculated values are smaller than the NON-SMOKER rates in the rest of the cases. For $^{52}$Fe the present rate exceeds the NON-SMOKER prediction above 2 GK and below this temperature it is less. On the other hand, our present calculation of astrophysical rates for the $(p,\gamma)$ reactions of $^{43}$V and $^{52}$Co merged with the NON-SMOKER calculation up to 2 and 1.5 GK, respectively. The difference between the two calculated rates increases with temperature for the $^{46}$V$(p,\gamma)$ reaction. It will be very interesting to see the effect of these rates in the abundance calculation of nuclei in relevant astrophysical environments.

## IV. SUMMARY

To summarize, we calculated the cross sections for $(p,\gamma)$ reactions in the mass range 40–54 in the relevant Gamow energy window appropriate for low energy astrophysical environments using the well-known reaction code TALYS1.6. Charge radii and binding energy values of various stable nuclei calculated using RMF theory have been compared in the mass region $A = 40$–54 with the available experimental data. The DDM3Y *NN* interaction is folded with target nuclear densities calculated from RMF to construct the optical potential which is needed for HF statistical model calculation and after proper normalization it has been used to verify the theory with the observed experimental data. The $(p,\gamma)$ reaction rates are calculated and plotted along with NON-SMOKER reaction rates. The main feature of our work is to place all the nuclei considered in the mass region $A = 40$–54 at the same footing and to use the same methodology for all of them to avoid systematic error.

## ACKNOWLEDGMENTS

The authors acknowledge the financial support provided by University Grants Commission, Department of Science and Technology, Alexander Von Humboldt Foundation, and the University of Calcutta.

[1] W. M. Howard, W. D. Arnett, D. D. Clayton, and S. E. Woosley, Astrophys. J. **175**, 201 (1972).
[2] D. D. Clayton and S. E. Woosley, Rev. Mod. Phys. **46**, 755 (1974).
[3] T. Rauscher and F. K. Thielemann, At. Data Nucl. Data Tables **75**, 1 (2000).
[4] T. Rauscher and F. K. Thielemann, At. Data Nucl. Data Tables **79**, 47 (2000).
[5] H. Schatz, Int. J. Mass Spec. **251**, 293 (2006).
[6] E. Bauge, J. P. Delaroche, and M. Girod, Phys. Rev. C **58**, 1118 (1998).
[7] E. Bauge, J. P. Delaroche, and M. Girod, Phys. Rev. C **63**, 024607 (2001).
[8] D. N. Basu, J. Phys. G: Nucl. Part. Phys. **30**, B7 (2004).
[9] D. N. Basu, P. Roy Chowdhury, and C. Samanta, Phys. Rev. C **72**, 051601(R) (2005).
[10] A. J. Koning, S. Hilaire, and M. Duizvestijn, in *Proceedings of the International Conference on Nuclear Data for Science and Technology, April 22-27, (2007), Nice, France*, edited by O. Bersillon, F. Gunsing, E. Bauge, R. Jacgmin, and S. Leray (EDP Sciences, Les Ulis, France, 2008), p. 211.
[11] S. Goriely, S. Hilaire, and A. J. Koning, Astron. Astrophys. **487**, 767 (2008).
[12] G. Gangopadhyay, Phys. Rev. C **82**, 027603 (2010).
[13] C. Lahiri and G. Gangopadhyay, Eur. J. Phys. A **47**, 87 (2011).
[14] C. Lahiri and G. Gangopadhyay, Phys. Rev. C **84**, 057601 (2011).
[15] C. Lahiri and G. Gangopadhyay, Phys. Rev. C **86**, 047601 (2012).
[16] S. Dutta, D. Chakraborty, G. Gangopadhyay, and A. Bhattacharyya, Phys. Rev. C **91**, 025804 (2015).
[17] D. Chakraborty, S. Dutta, G. Gangopadhyay, and A. Bhattacharyya, Phys. Rev. C **91**, 057602 (2015).
[18] B. G. Todd-Rutel and J. Piekarewicz, Phys. Rev. Lett. **95**, 122501 (2005).
[19] M. Bhattacharya and G. Gangopadhyay, Phys. Rev. C **72**, 044318 (2005).
[20] M. Bhattacharya and G. Gangopadhyay, Fiz. B **16**, 113 (2007).
[21] A. Bouyssy, J.-F. Mathiot, N. Van Giai, and S. Marcos, Phys. Rev. C **36**, 380 (1987).
[22] P. Quentin, in *Nuclear Self-Consistent Fields*, edited by G. Ripka and M. Porneuf (North-Holland, Amsterdam, 1975), p. 297.
[23] A. M. Kobos, B. A. Brown, R. Lindsay, and G. R. Satchler, Nucl. Phys. A **425**, 205 (1984).
[24] A. K. Chaudhuri, Nucl. Phys. A **449**, 243 (1986).
[25] A. K. Chaudhuri, Nucl. Phys. A **459**, 417 (1986).
[26] G. R. Satchler and W. G. Love, Phys. Rep. **55**, 183 (1979).
[27] G. Bertsch, J. Borysowicz, H. McManus, and W. G. Love, Nucl. Phys. A **284**, 399 (1977).
[28] W. D. Myers, Nucl. Phys. A **204**, 465 (1973).
[29] R. R. Scheerbaum, Nucl. Phys. A **257**, 77 (1976).
[30] J. J. Cowan, F.-K. Thielemann, and J. W. Truran, Phys. Rep. **208**, 267 (1991).
[31] J. A. Holmes, S. E. Woosley, W. A. Fowler, and B. A. Zimmerman, At. Data Nucl. Data Tables **18**, 305 (1976).
[32] A. J. Koning, S. Hilaire, and S. Goriely, Nucl Phys. A **810**, 13 (2008).
[33] S. Goriely, Phys. Lett. B **436**, 10 (1998).
[34] S. Goriely, N. Chamel, and J. M. Pearson, Phys. Rev. Lett. **102**, 152503 (2009).
[35] C. Iliadis, *Nuclear Physics of Stars* (Wiley-VCH, Weinheim, 2007).
[36] A. Parikh, J. José, F. Moreno, and C. Iliadis, Astrophys. J. Suppl. Ser. **178**, 110 (2008).
[37] O. Koike, M. Hashimoto, R. Kuromizu, and S. Fujimoto, Astrophys. J. **603**, 242 (2004).
[38] H. Schatz, A. Aprahamian, V. Barnard, L. Bildsten, A. Cumming, M. Ouellette, T. Rauscher, F.-K. Thielemann, and M. Wiescher, Phys. Rev. Lett. **86**, 3471 (2001).
[39] J. L. Fisker, H. Schatz, and F.-K. Thielemann, Astrophys. J. Suppl. **174**, 261 (2008).
[40] T. Rauscher and F.-K. Thielemann, in *Stellar Evolution, Stellar Explosions, and Galactic Chemical Evolution*, edited by A. Mezacappa (IOP, Bristol, 1998), p. 519; arXiv:nucl-th/9802040.
[41] H. De Vries, C. W. De Jager, and C. De Vries, At. Data Nucl. Data Tables **36**, 495 (1987).
[42] M. Wang, G. Audi, A. H. Wapstra, F. G. Kondev, M. MacCormick, X. Xu, and B. Pfeiffer, Chin. Phys. C **36**, 1603 (2012).
[43] I. Angeli, At. Data Nucl. Data Tables **87**, 185 (2004).
[44] M. Bhattacharya and G. Gangopadhyay, Phys. Lett. B **672**, 182 (2009).
[45] G. Gangopadhyay, J. Phys. G : Part. Nucl. Phys. **37**, 015108 (2010).
[46] M. E. Sevior, L. W. Mitchell, C. I. W. Tingwell, and D. G. Sargood, Nucl. Phys. A **454**, 128 (1986).
[47] F. M. Mann, Hanford Engineering and Development Lab. Report HEDL-THE-76-80, 1976 (unpublished).
[48] J. L. Zyskind, C. A. Barnes, J. M. Davidson, William A. Fowler, R. E. Marrs, and M. H. Shapiro, Nucl. Phys. A **343**, 295 (1980).
[49] S. E. Woosley, W. A. Fowler, J. A. Holmes, and B. A. Zimmerman, Atomic Data and Nucl. Data Tables **22**, 371 (1978).
[50] S. R. Kennett, L. W. Mitchell, M. R. Anderson, and D. J. Sargood, Nucl. Phys. A **363**, 233 (1981).
[51] S. E. Woosley, W. D. Arnett, and D. D. Clayton, Astrophys. J. Suppl. **26**, 231 (1973).
[52] A. E. Vlieks, C. W. Cheng, J. D. King, Nucl. Phys. A **309**, 506 (1978).
[53] L. W. Mitchell, M. R. Anderson, S. R. Kennett, and D. G. Sargood, Nucl. Phys. A **380**, 318 (1982).
[54] S. R. Kennett, Z. E. Switkowski, B. M. Paine, and D. G. Sargood, J. Phys. G: Nucl. Phys. **5**, 399 (1979).
[55] J. L. Zyskind, J. M. Davidson, M. T. Esat, R. H. Spear, M. H. Shapiro, William A. Fowler, and C. A. Barnes, Nucl. Phys. A **315**, 430 (1979).
[56] G. A. Krivonosov, O. I. Ekhichev, B. A. Nemashkalo, V. E. Storizhko, and V. K. Chirt, Izv. Rossiskoi Akademii Nauk, Ser. Fiz. **41**, 2196 (1977).
[57] H. J. Gardner, L. W. Mitchell, S. R. Kennett, M. R. Anderson, and D. G. Sargood, Aust. J. Phys. **34**, 25 (1981).
[58] J. L. Zyskind, J. M. Davidson, M. T. Esat, M. H. Shapiro, and R. H. Spear, Nucl. Phys. A **301**, 179 (1978).
[59] W. A. Fowler, J. Powelson, B. A. Zimmerman, and S. E. Woosley (private communication).
[60] S. R. Kennet, L. W. Mitchell, M. R. Anderson, and D. G. Sargood, Nucl. Phys. A **368**, 337 (1981).
[61] M. A. Famiano, R. S. Kodikara, B. M. Giacherio, V. G. Subramanian, and A. Kayani, Nucl. Phys. A **802**, 26 (2008).

[62] S. R. Kennett, M. R. Anderson, Z. E. Switkowski, and D. G. Sargood, Nucl. Phys. A **344**, 351 (1980).
[63] S. R. Kennett, M. R. Anderson, L. W. Mitchell, and D. G. Sargood, Nucl. Phys. A **346**, 523 (1980).
[64] http://nucastro.org/nonsmoker.html.
[65] F.-K. Thielemann, M. Arnould, and J. W. Truran, *Advances in Nuclear Astrophysics*, edited by E. Vangioni-Flam (Gif sur Yvette: Editions Frontieres, 1987), p. 525.
[66] J. R. Nix, W. D. Myers, and W. Swiatecki, At. Data Nucl. Data Tables **59**, 185 (1995).
[67] See Supplemental Material at http://link.aps.org/supplemental/10.1103/PhysRevC.94.015802 for numerical values of calculated reaction rates.